Memoirs of the Faculty of Science, Kyoto University, Series of Physics, Astrophysics, Geophysics and Chemistry, Vol. XXXII, No. 1. Article 1, 1967.

THE 60-CENTIMETER EQUATORIAL REFLECTOR AT THE KWASAN OBSERVATORY

BY

Yoshihiro NAKAI

(Received April 18, 1967)

ABSTRACT

General features of the Kwasan Observatory's 60-cm reflector are briefly described. Methods of the optical testing and adjusting are discussed for a reference of wide use.

Optical qualities of the mirror system are estimated. Final Hartmann-constant is T=0.17.

§1. Introduction

In October 1960, as has been introduced by Miyamoto [1], 60-cm reflector for planetary observations was installed at the Kwasan Observatory, University of Kyoto, after four years' planning-, designing-, and constructing stages.

Just for the reason to meet the 1960 Mars opposition [2], final figuring of the mirrors has been suspended, temporarily, but since that time, several series of the international co-operation for Moon-watch (with the University of Manchester (England) and NASA-ACIC (USA) group by Kopal, 1962–65) [3] and for Venus (with Pic-du-Midi (France) group by Dollfus 1964) started. Testing and refiguring were postponed until series of above observations were closed. In this paper, we briefly describe the general features and the quality of this telescope.

§2. General Features

The main mirror is 60-cm in diameter and 330-cm in focal length, and focal-ratio, F/5.5.

Prime focus, 2 Newtonian foci and Cassegrainian focus are available. Cassegrainian focal length is 1200-cm and F/20. The Cassegrainian hyperboloid mirror and Newtonian diagonal flat mirror are easily able to set at its own position below the prime focus with three supporting fins. The Cassegrainian mirror can be removed and interchangeable with the prime focus camera or the Newtonian diagonal flat mirror within 5 minutes.

Guiding telescope is a refractor of 15-cm aperture and F/16.

As illustrated in Plate 1 and Fig. 1, mouting is a traditional German type. To rotate the axes both in Declination and Right-Ascension, precisely, weight-free cylindrical axis and loaded axis are applied to the Declination axis, and loaded rollers to the Right-Ascension axis.

Telescope tube is simple frame-works of high-tension steel.

Quick setting to Right-Ascension- and Declination-position can be operated by

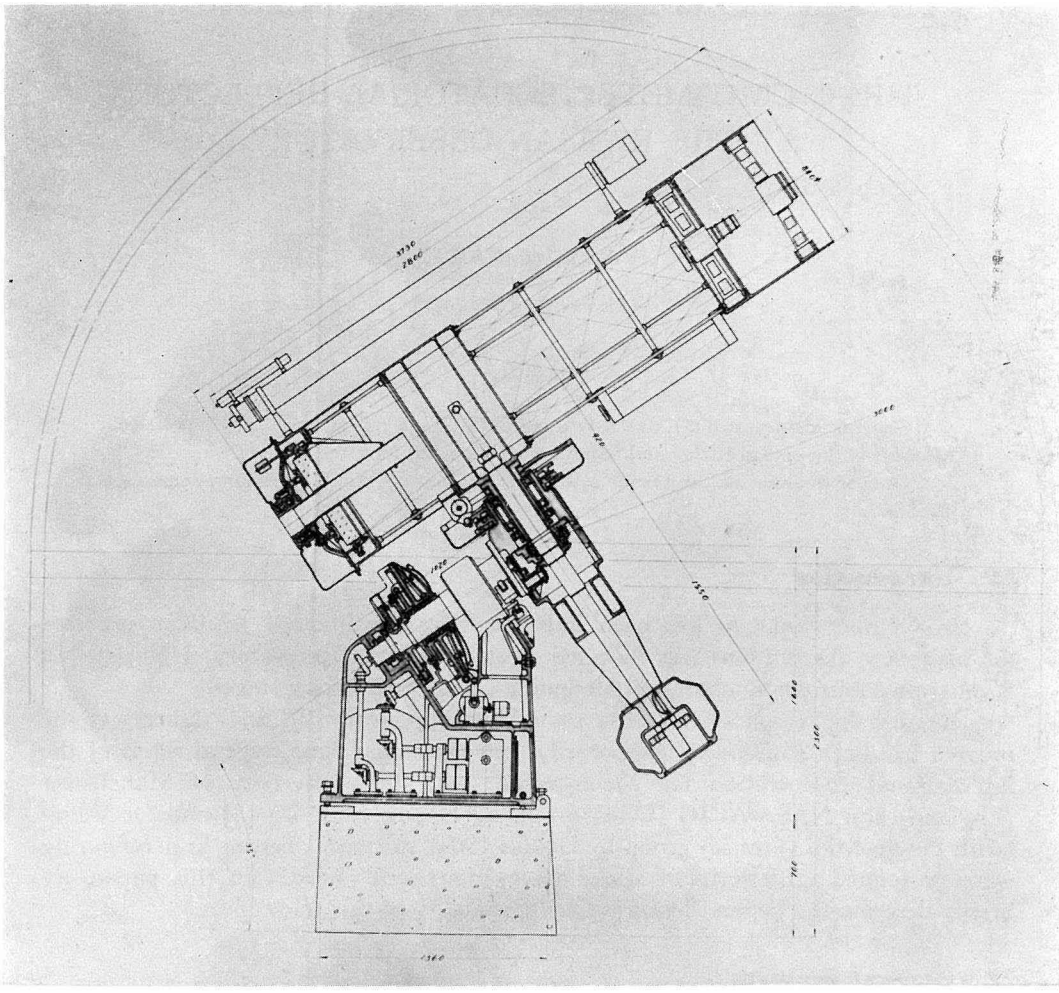

Fig. 1. Section of 60-cm reflector at the Kwasan Observatory.

a wheel at the west side of pier, and other operations are electrically remote controlled at any observer's position. Driving and control system is shown in Fig. 2.

§3. Optics

The main mirror is 60-cm in diameter and has a 18-cm hole at the center. It is ground and polished in a form of paraboloid of 330-cm in focal length. Practically, wide field photographs are taken at the prime focus of this mirror. Cassegrainian mirror has a effective diameter of 17-cm and yields a composite focal length of 1200-cm (4). The converging light beam reflected on this mirror passes through the center hole of main mirror and focuss on a plane about 52-cm back from the front surface of main mirror. This means that the back-focus from Cassegrainian mounting-flange is 15-cm (see Fig. 3).

In order to photograph the full-size of the moon at Cassegrainian focus, all the

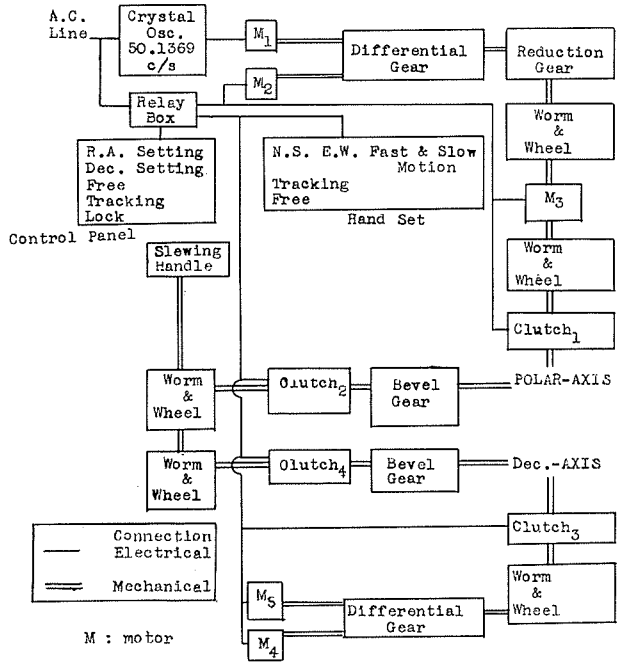

Fig. 2. Block diagram of driving and control systems.

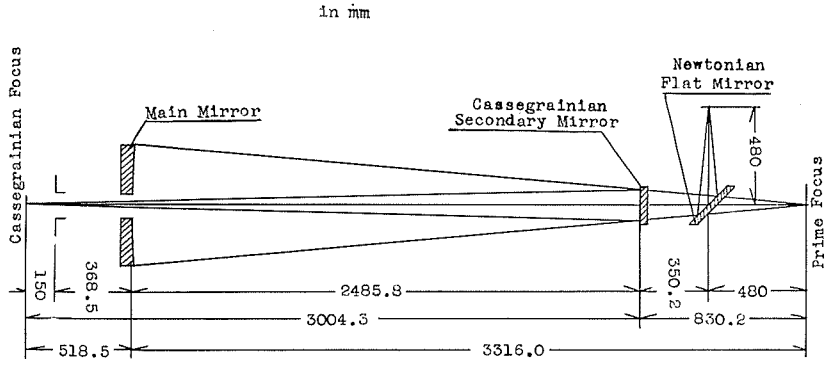

Fig. 3. Optical arrangements.

size of secondary mirror, sky-buffle, and light-shield is adopted not to vignette the field of view of 17-minutes of arc.

The main mirror is of low-expansion-coefficient Chance-Pilkington glass (O–W–2), which has a coefficient of thermal expansion $30\sim35\times10^{-7}/°C$, and other optical parts are of the Corning Pyrex.

§4. Mirror Supports, and Systems

The mirror should be defined within close limits and retained its shape in all

positions within satisfactory limits of $\lambda/12$ as described in §6, yet be free from any strains.

The thickness of main mirror is 97-mm, and then thickness ratio to diameter is 1/6.2. When we assume the elastic modulus 6200 and specific gravity 2.25, axial supports of nine points satisfactorily sustain the solid disk of thickness ratio 1/6.2 without surface deformation more than $\lambda/12$, in horizontal position [5]. For the case of our 60-cm main mirror under the condition above mentioned, we can safely sustain the whole weight of the mirror with 18 pads, without surface deformation more than $\lambda/12$.

Axial Support: In Plate 2, axial support arrangements of 18 mirror back pads are shown. The 18 back pads transmit the mirror's weight to the point-contact rolling surfaces on the 6 tripods, and successively these weights are transmitted by 6 point-contact rolling surfaces to 3 seasaw levers. These levers are connected at their centers to backside of cell through 3 back-support screws, and collimating is done by these three screws.

Each pad is free to adjust in angle about the ball to align it against the mirror, and also free to move parallel to the mirror-back to allow for differential thermal expansion between the solid disk of glass and steel cell. These universal joints have retainers to prevent the pads to drop.

Lateral Support: The steel band with high compression rubber lining, is bound to the lateral of the mirror. The steel band and lateral supporting units are illustrated in Plate 3. A lateral supporting unit consists of a push-rod with a ball, an adjusting-screw, a lever and a counter-weight. These 12 units, spaced at intervals of 30°, can support the center of gravity and balance the gravitational components of mirror-weight at any tilting of cell..

The position of the mirror is defined by three push-rods located at intervals of

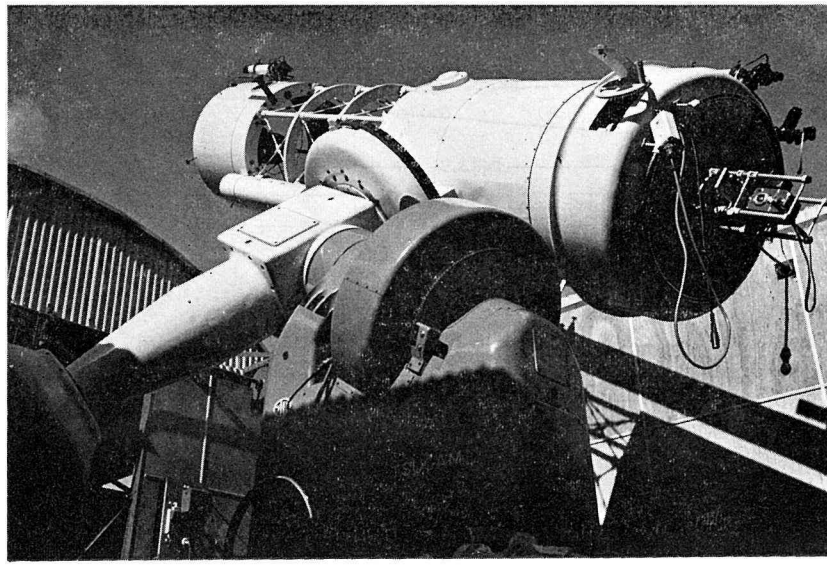

Plate 1. General view of 60-cm reflector.

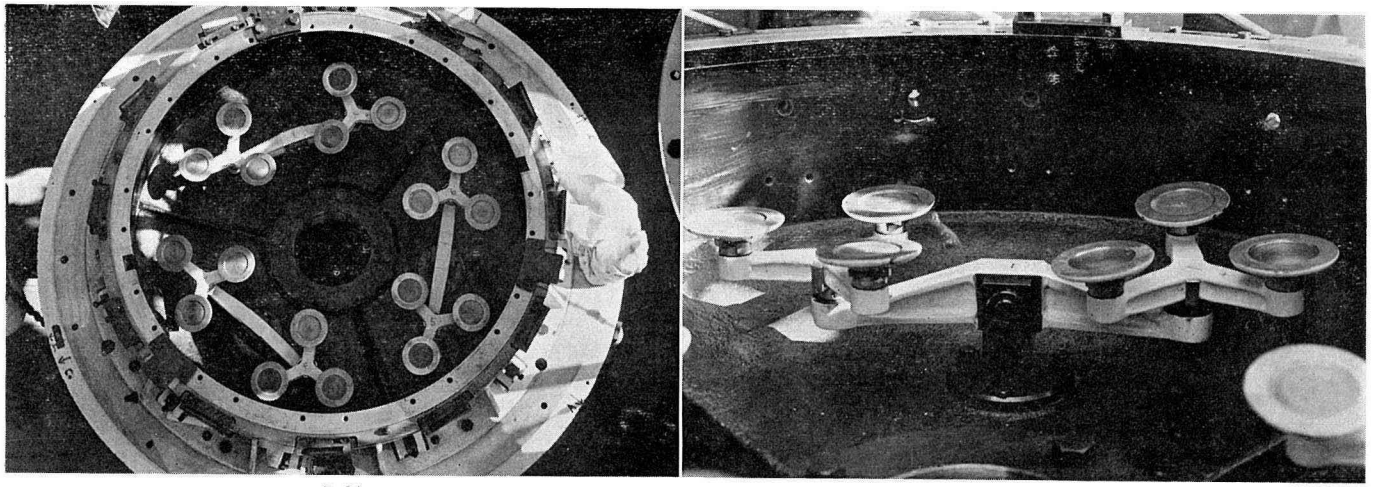

(left) (right)

Plate 2. Axial support system. The lay-out of 18 pads (left) and close-up of unit (one of three) (right)

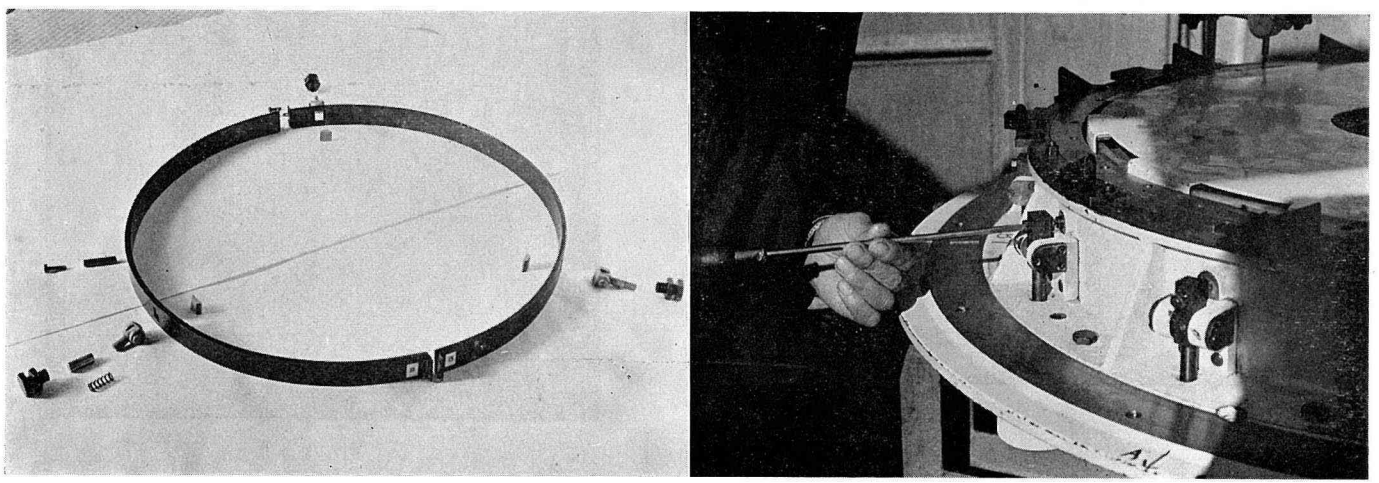

(left) (right)

Plate 3. The steel band and push-rods (left) and lateral support system (right). Each unit consists of adjust-screw, lever and counter-weight.

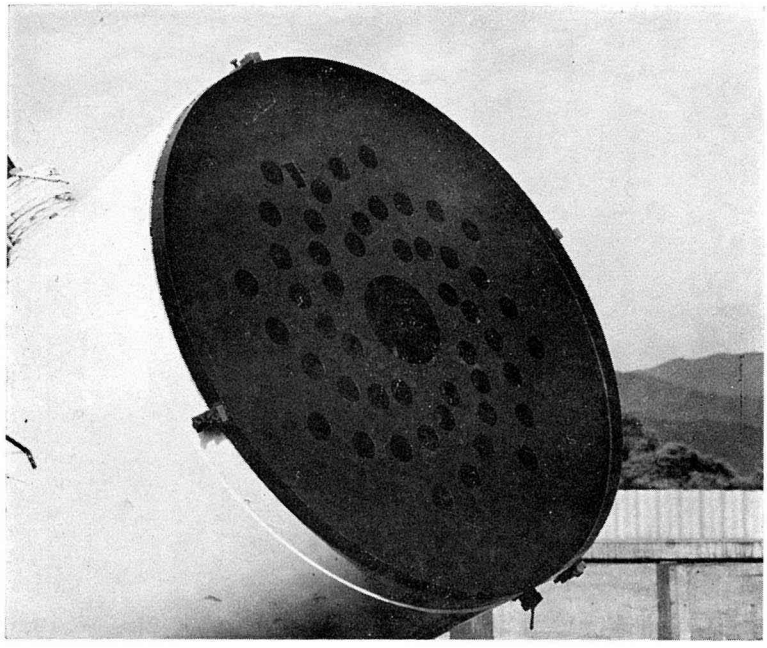

Plate 4. Hartmann-screen mounted on the telescope.

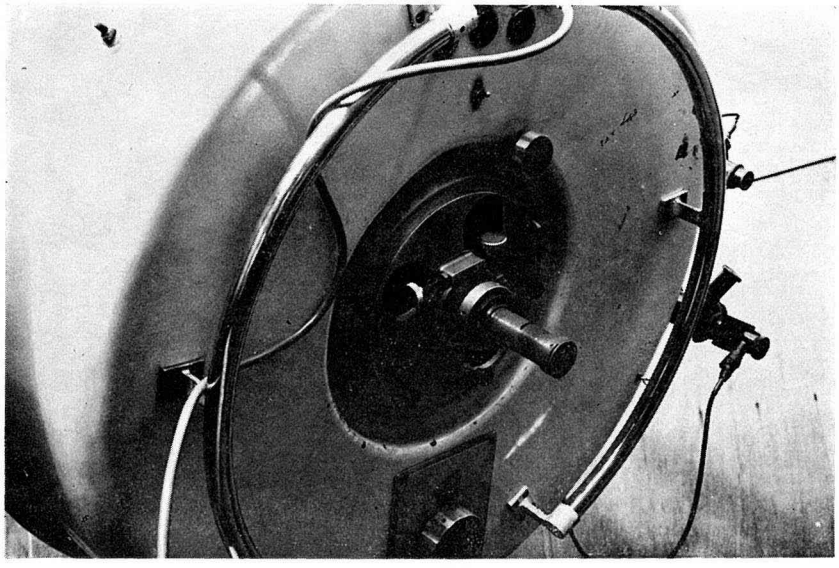

Plate 5. Simple plate-holder attached at Cassegrainian focus.

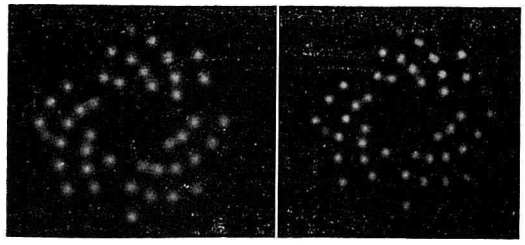

Plate 6. Reproductions of Hartmann-screen images of Aug. 3, 1966. Left is inside and Right outside. (about 6 times enlarged).

120°. These push-rods are made of poly-vinyle-chloride in our case. The expansion-coefficient of materials and length of push-rods should be chosen to compensate the lateral differential thermal expansion between the solid disk of glass and steel cell. These push-rods transmit the force to the mirror directly through the windows on the band as shown in Plate 3 (left). Poly-vinyle-chloride rod is not so rigid as steel, and the push-rods define the position of mirror under the weight-free condition depending on lateral system. The center is decided by these heads of 3 poly-vinyle-chloride push-rods with reference to the cell.

Although the differential thermal expansion in axial component is very small, the differential motion may cause the strain by the friction between poly-vinyle-chloride push-rods and pads: band surface should be normal to steel push-rods, if not, these rods bind up the motion and may cause some strain.

§5. Optical Alignment

The alignment of Cassegrainian optical axis is achieved by putting the vertexes and main axes of mirrors on the line of sight which should be identical with the axis of Cassegrainian focus-mount, and vertical to mount flange at its center. The squaring of prime- or Newtonian-focus camera is also achieved by adjusting the plate in plate-holder at right-angle to the line of sight by squaring adjust-screws. These procedures are done practically as follows:

(1) Set an auto-collimater at the Cassegrainian focus-mount and fix up center-marking as the indicator of the line of sight (or mechanical center).
(2) Point a star on center-marking through the auto-collimater without secondary mirror, and read off the angular distance and position of the star image of main mirror on the ground glass at the prime focus to the center-marking through the auto-collimater.
(3) Tilt the main mirror against the cell and bring the image onto center-marking.
(4) Repeat the practice to get fine alignment.
(5) Stretch thin-wires on two diagonal diameters of secondary mirror cell. Cross-point of the wires will indicate approximately the vertex of the Cassegrainian hyperboloid or the mechanical center of secondary mirror cell.
(6) Adjust the lateral position of the secondary mirror cell and set the cross-point on the center-marking through the auto-collimater. Then the vertex of secondary mirror is on the line of sight.
(7) Tilt the seeondary mirror cell until the reflected light images on the secondary

mirror, from 4 light sources separated on a circle in 90° around the auto-collimater, concentrate onto cross-point of the wires.

(8) Repeat (6) and (7) to get fine alignment. Then the alignment of Cassegrainian optical axis is achieved. And squaring of Cassegrainian mount is not needed except for mechanical cares of each attachment.

(9) Adjust the squaring screws to set the flat glass plate in plate-holder set on the prime- or Newtonian camera at right-angle to the axis of auto-collimater.

Accuracy of this method of collimation is due to the accuracy of auto-collimater, mechanical accuracy of cells including Cassegrainian mount and limits of detection of errors with artificial light by eye. In our case, a little adjustment of tilting of secondary mirror is applied by the method using the inner- and outer-focus image of a star.

§6. Optical Qualities

Main Mirror: During the works of polishing and figuring of the main mirror, we tested the longitudinal aberration frequently for the various zones, and constructed the actual shape of the surface refering to the paraboloid given by equation (1):

$$\sum h = -\sum \Delta D \cdot y \cdot d \cdot R^{-2}, \tag{1}$$

where h is the deviation between the actual and theoretical paraboloid across a zone of width d, and y is the radius of the zone, and ΔD is the difference between the observed longitudinal aberration and theoretical value ($y^2/2R$) i.e. residual longitudinal aberration. R is the radius of the reference sphere. Summation is carried out over the zone from center to edge, so $\sum h$ is the actual shape of mirror referred to paraboloid. The zonal test was carried out visually with Foucault tester which was designed to eliminate the parallax. As pointed out by Platzeck and Gaviola [6], this method has the disadvantage of asymmetry so far as the knife-edge is used, but has the advantage o fsimplicity. The disadvantage of this method is improved by cutting the light beam with thin wire instead of the knife-edge and determining y on the photographic plate taken at expected position. The accuracy of the knife-edge method is satisfactorily within $\lambda/50$ for each zone of inner area, and the wire method for outer area. A series of final test was carried out by these two methods alternatively, in the carefully air-conditioned Solar Laboratory at Kwasan, and measurements were analized and calculated to confirm the accuracy within $\lambda/12$ over the whole surface by the author [7]. $\Delta D = f(y)$ i.e., residual longitudinal aberration and $\sum h$ are shown in Fig. 4. Summation is calculated with zonal width of 30-mm and within accuracy of $\lambda/12$. Accuracy of $\lambda/12$ over the whole surface of mirror is the tolerance to get the good image containing the light within phase difference of $\lambda/4$ recommended by Rayleigh, by the combination of main- and Cassegrainian secondary-mirrors with equal precision.

When the filler of Pyrex cemented in center hole is removed, strains may be released and deformation of the mirror surface should happen. Actually, surface is too concave inside (y: 70 ^{mm}~120 ^{mm} i.e. about 900 Å,) and turns up outside (y: 240 ^{mm}~300 ^{mm} i.e. about 400 Å) as illustrated in Fig. 4.

After all, we decided that local retouching is not necessary, by the following reasons:

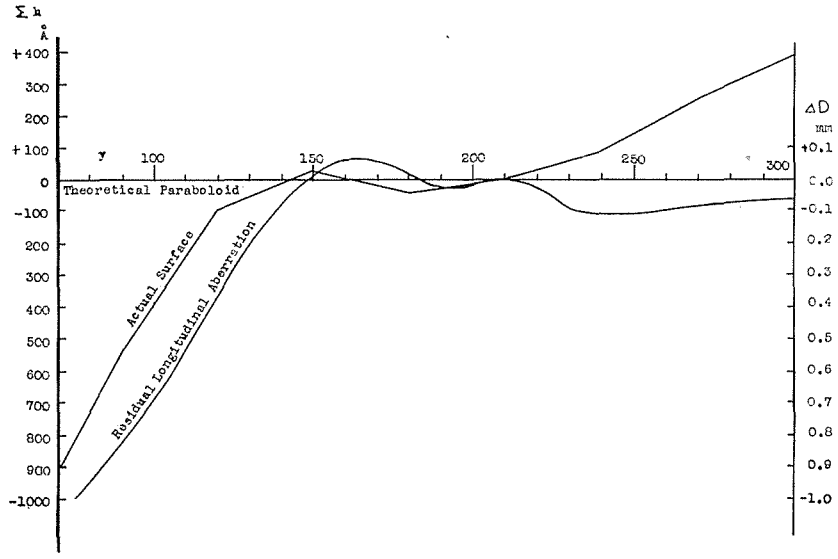

Fig. 4. Residual longitudinal aberration by the knife-edge and thin- wire method, and actual surface of the 60-cm mirror.

1) It is very difficult to smooth out the residuals with small tool only, without center filler.
2) The radius of the circle of least confusion, calculated by equation (2), is 3.4 μ at the focus and is less than the linear scale of theoretical resolving power of 3.8 μ:

$$\overline{\rho} = \sum y^2 \cdot \Delta D / 2 \cdot f \cdot \sum y \,. \qquad (2)$$

Where f is the focal length of the main mirror.
3) Prime focus camera is vignetting inner circle of diameter of 20-cm, and reflected light from the main mirror (y: 100 mm~300 mm) in use has phase difference of 1600 Å ($=\lambda/3.4$) at prime focus. And this value is nearly equal to the Rayleigh's criterion of $\lambda/4$.
4) Above mentioned conditions 2) and 3) nearly satisfy the criteria for spherical aberration by Danjon and Couder [8].

Cassegrainian mirror: Cassegrainian hyperboloid convex-mirror is figured by comparing with master concave hyperboloid by interference method, and some corrections are applied to compensate the errors of the main mirror. The master hyperboloid concave-mirror is tested by longitudinal aberration method. The interference method is not so severe to test such aspherical mirror within accuracy of $\lambda/12$, and inferior to the longitudinal aberration method. So, this method is applied only to see the tendency of curvature, and finally Hartmann's test [9] is adopted.

The Hartmann's test at Cassegrainian focus: The Hartmann screen used to obtain the test plates is shown in Plate 4, and the pattern of holes, in Fig. 5. The Hartmann screen is made of 1-mm steel sheet, and considerable care is paid to locate the position of holes within 0.05-mm, and the center of the screen is set on the line

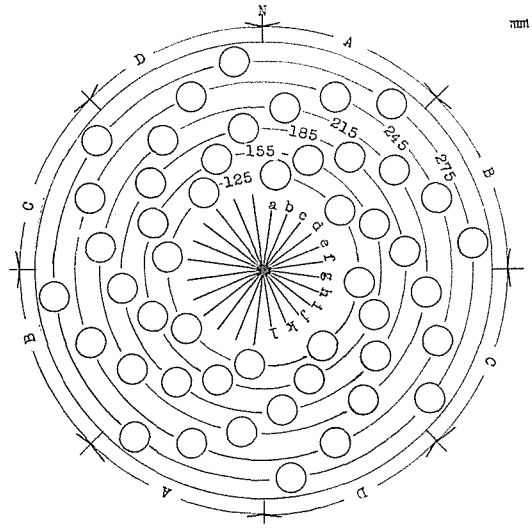

Fig. 5. The Hartmann-hole pattern. The numbers are the radius of zones represented by holes.

of sight by auto-collimater. The 40-mm-ϕ holes ($f_c/300$) are drilled 50-mm apart on 24 radii that are spaced 15° in position angle. Holes on successive radii are staggered and the central distance differs by 30-mm on adjacent radii.

All the test plates were taken at the Cassegrainian focus with the simple apparatus i.e. a cylindrical camera illustrated in Plate 5. To take the Hartmann photographs, an average focus position was visually, at first, decided with the knife-edge. Two slots are separated 200-mm apart on cylindrical camera, and can hold the plate 100-mm inside or outside from the average focus with an accuracy of 0.01-mm. The plate size is 30×30 mm^2, and plate is loaded into a slot without shelter and clamped by screws.

Plate 6 is a reproduction of the pair of the Hartmann plates of August 3, 1966. The emulsion is Oriental A–1, and it photographs α Cygni with 10-sec. exposure. Some of the images are affected by the prime-focus camera and supporting fins.

In order to detect the aberrations, the distance of the images from mean center should be measured on inside- and outside-plates as illustrated in Fig. 6. Distances of a_1', a_1'', a_2' and a_2'' are measured for a pair of symmetrical holes.

Now traditional Hartmann's constant is defined as follows:

$$T=\frac{200000}{f}\cdot\frac{\sum y\cdot\rho}{\sum y}\,. \tag{3}$$

In this expression, ρ is the half of the distance between the images of the two symmetrical holes at radius y on a plane in the mean focus:

$$\rho=\frac{y\,|d_1-\bar{d}|}{f}\,,$$

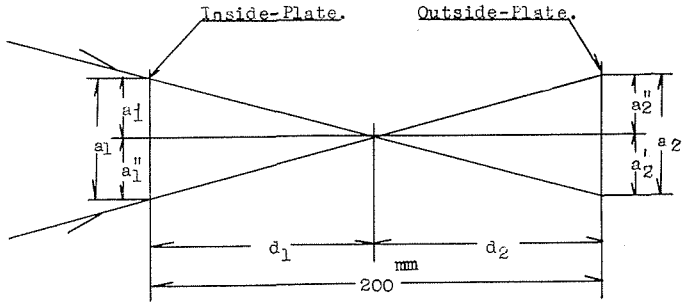

Fig. 6. A section through the optical axis at focus. Inside and outside plates, and light bandle from a single pair of holes on one diameter are shown.

where $\bar{d}$ (distance from inside plate emulsion to the mean focus)

$$\bar{d} = \frac{\sum y \cdot d_1}{\sum y},$$

and

$$d_1 = \frac{a_1(d_1+d_2)}{a_1+a_2}.$$

Hartmann's constant, for our case, is $T=0.17$.

We can trace the variation of $(d_1-\bar{d})$ along the radius on different sections of the mirror. Fig. 7 shows the results for Sections A, B, C, and D (see Fig. 5), and their mean value T. The amount of astigmatism may be obvious. Of course, this includes contributions due to collimating error as well as essential one. This result is useful in the figuring process of Cassegrainian secondary mirror. In our case, some corrections to the shape of secondary mirror to compensate the errors of main mirror seem to be satisfactorily adopted, as seen in later numerical examples.

Fig. 7. Spherical aberrations obtained by Hartmann-test on Aug. 3, 1966.

In the calculations above mentioned, we assumed that the lights from the symmetrical holes converge symmetrically, but practically light beams are affected by local irregularity on the mirrors, and scatter in the radial and tangential directions asymmetrically. In this paper, we deal with radial components in asymmetry and neglect tangential ones [10].

When we consider asymmetrical deflection, the distance δ of image from mean center in the focal plane is determined by

$$\delta = a_1' - \frac{\bar{d}}{d_1+d_2}(a_1'+a_2') \ . \tag{4}$$

Geometry is also shown in Fig. 6.

Substituting ρ in eq. (3) by δ of eq. (4), and 200000 by 206265, we can get more practical quantity of the radius of a circle of least confusion in second of arc,

$$T'' = \frac{206265}{f} \cdot \frac{\sum y \cdot \delta}{\sum y} \ . \tag{5}$$

For our case, we have

$$T'' = 0.''22 \ .$$

Our estimated values for T and T'' are less than the radius of the circle of the theoretical diffraction disk of 0.″23 for 60-cm diameter.

Fig. 8 shows "scatter diagram" of light beams from each holes (36 points of measurement) at the focus. The light flux of light beam from Hartmann hole which

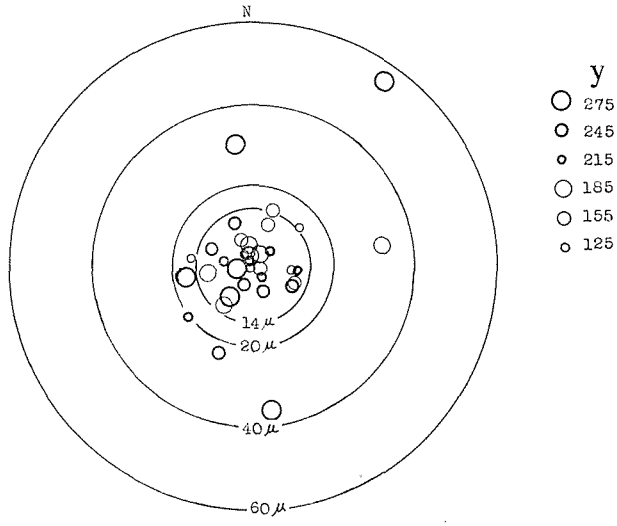

Fig. 8. Scatter diagram, on the focus, (Aug. 3, 1966).

represents a zone is proportional to y of each zone, and distance from the center is taken as δ. If the amount of light ($\sum y$) within the various zones of the image is divided by the area of these zones which is proportional to the mean radius of zones, the distribution of intensity within the image is obtained. And also, the relative light flux falling within each zone can easily be computed by counting the $\sum y$. This distribution and light flux are shown in Fig. 9. The relative light flux is represented in a histogram: solid curve shows the smooth run of intensity distribution within the Cassegrainian image. The intensity drops to one-half the maximum at a distance of 12 μ from the center. The broken-line histogram shows the relative light flux in % within image diameter of 0~60 μ: intervals of 5 μ are used. Within the radius of 25 μ, 85% of total light flux are concentrated.

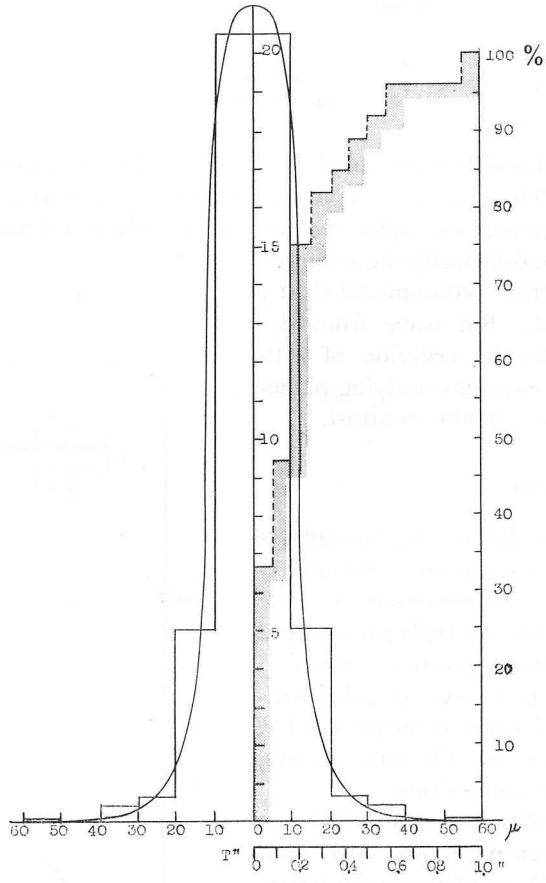

Fig. 9. Intensity distribution and light concentration.

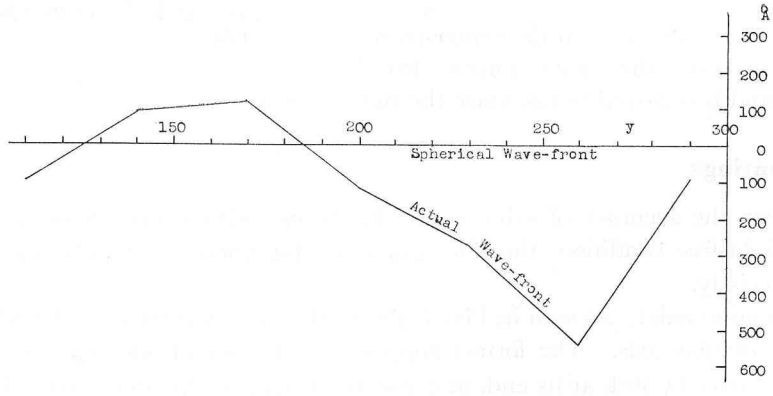

Fig. 10. Half-profile of wave-front at the focus, (Aug. 3, 1966).

The difference between the actual wave front and ideal wave front of sphere is given by

$$\sum X_y = \frac{-1}{f^2} \sum (d_{1i} - \bar{d}) y \cdot d \,, \qquad (6)$$

where d is the zonal width represented by central radius of y, and the results are shown in Fig. 10. The maximum deviation is apparently within 660 Å ($\lambda/8.3$).

From these numerical examples, we can say that the our Cassegrainian optical system would have satisfactorily the accuracy for a good objective recommended by Danjon and Couder. But wave front deviation is inferior to the criterion of $\lambda/16$ recommended by Francon for studying planetary detail of minimum visible contrast.

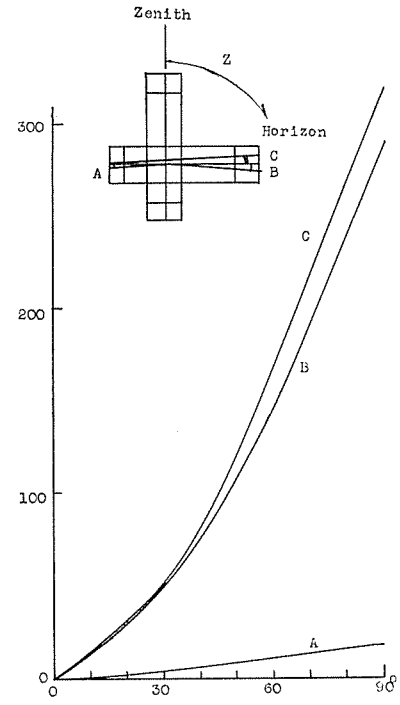

Fig. 11. Deflection of the telescope tube.

§7. Telescope Tube

As shown in Fig. 1, the telescope tube is simple frame-works and connects the upper-tube and lower-cell to the center-piece. The frame-works are made of high-tension-steel as chord members (upper has 6 and lower 8) and Hisatsune-cast-steel rings as web members, and minor steel struts as the pre-loader. The pre-loader compresses the tube axially, and improves the strength of tube.

The accuracy of parallelism and deviation of centers between upper and lower ends of tube are within 20-sec. of arc, and 0.5-mm, at zenith-distance of 0°, respectively.

The deflection of actual tube is illustrated in Fig. 11, as a function of zenith-distance.

The dew-cover between the center-piece and cell protects the main mirror from moisture, and is removed to minimize the tube current.

§8. Mountings

To keep the accuracy of driving, the driven axes with worm-wheel are kept in nearly weight-free condition, therefore gears are interlocked smoothly and can be rotated precisely.

Declination axis: As seen in Fig. 1, the Declination axis consists of loading axis and outer tubular axis. The former supports the weight of telescope tube at the center of gravity by fork at its end, and counter-weight at the other end. This axis is supported at the center of gravity (cross point of Dec. and R.A. axes) by self-aligning ball-bearings as gimbals. The bending due to loading on either side is absorbed

in counter-weight side. The live axis of Declination can support the telescope tube as weight-free condition precisely without bending, and worm-and-wheel interlocks smoothly. The displacement and deflection around the rotational axis are within 5 μ and 7 sec. of arc, respectively.

Right Ascension Axis: The polar axis is supported by two ball-bearings at both ends and by thrust-bearing at lower end. At the upper end close to the Declination axis two rollers push up the almost all the weight of movable parts. The force of pushing up is adjustable with micrometer-screw to compensate the increase and decrease of weight of movable parts due to the interchange of accessary. This system can serve for stable rotation of axis i.e. smooth interlock and precise driving. The displacement and deflection around the polar-axis are 5 μ and 3 sec. of arc, respectively.

§9. Driving and Controls

The Right-Ascension-drive consists of a double worm-wheel and a bevel gear system. The bevel gear system is operated by hands for slewing the telescope and the others for tracking, guiding and setting. The Declination-drive consists of a single worm-wheel and bevel gear system, and these are operated as Right-Ascension operated.

The Right-Ascension worm-wheel has a diameter of 80-cm with 800 teeth which is driven by a worm having a diameter of 5-cm. The maximum tooth-to-tooth accuracy of worm-wheel and worm are 3.4 μ and 1.5 μ. The mechanical accuracy obtained are shown in Table 1.

Table 1. The mechanical accuracy obtained.

Errors	Right Ascension	Declination
Errors of Rotation		
Deflection	3″	7″
Displacement	1.5 μ	5 μ
Errors of Worm		
Tooth-to-Tooth	1.5 μ (0.7)	25 μ
End-Play	0.5 μ (0.2)	1 μ
Errors of Worm-Wheel		
Tooth-to-Tooth	3.4 μ (1.7)	11 μ
Accumulated	8.1 μ	38 μ
Centering	10 μ	14 μ

The driving worm has a axial motion restrained by ball-point-contact which is loaded by coaxal coil spring, and the end-play is within 0.5 μ. The tracking mechanism is constructed to satisfy the specification that the local errors should not exceed 0.2 sec. of arc per 10 seconds. The driving and control systems are shown in Fig. 2.

The rotation is transmitted by clutch which is clamped by springs in tracking time when the electric current is controlled to be off. And the clamp-spring-pressure is adjusted so that, in case of emergency overload, the clutch-facings are allowed to begin slipping.

The telescope drive constants are as follows:

Slewing rate	:	3°/1 rotation of handle.
Setting rate	:	45′/min.
Guiding rate	:	30″/min.
Tracking Accuracy	:	0.2″/10 sec. at sidereal rate.

§10. Conclusion

Traditional Hartmann's constant T for the representation of optical qualities has not physical meaning. For the estimation of optical qualities, T'' calculated by eq. (5), light concentration shown by Fig. 8 and 9 and wave-front error by eq. (6) may serve better.

In the process of figuring main mirror and optical alignment, Herschelian aberration should be eliminated.

Criteria recommended by this author for a good telescope for the planetary works are as follows:

1) Calculated value of T'' should be less than the radius of the circle of the theoretical diffraction disk of the telescope.
2) Wave-front error, $\sum X_y$, should be less than $\lambda/16$.
3) Tracking error within the expected longest exposure for planetary works without manual adjustment should be less than the resolving power.

In our case, we have $T'' = 0''.22 < 0''.23$, $\sum X_y = \lambda/8 > \lambda/16$ and tracking error $< 0''.2/10$ sec..

Acknowledgement

The author wishes to express his deepest thanks to Director Prof. Shotaro Miyamoto for his encouragements and valuable advices throughout the period of designing, construction and testing. He also thanks to Mr. Taisuke Tsugami, President of the Tsugami Precision Works Co., who has been generous to support this works. During our works, we were supported by many people, and without their aid 60-cm reflector could not be brought into completion.

REFERENCES

[1] S. Miyamoto, Sky and Telescope, **21**, No. 2, p. 90~91, 1961.
[2] S. Miyamoto & Y. Nakai, Contr. Inst. Astrophys. & Kwasan Obs., No. 105 1961.
[3] S. Miyamoto & A. Hattori, Ibid, No. 137, 1964 .
[4] Y. Nakai, The Heavens, **47**, 498, p. 290~295, 1966. (In Japanese)
[5] D. Maksutov, Technologie der Astronomischen Optik, p. 62~66, 1954, VEB Verlag Technik BERLIN.
[6] R. Platzeck & E. Gaviola, J.O.S.A., **29**, p. 484~489, 1939.
[7] Y. Nakai, The Heavens, **48**, 506, p. 185~189, & **48**, 507, p. 216~223, 1967. (In Japanese)
[8] A. Danjon & A. Couder, Lunettes et Télescope, p. 522, 1935, Editions de la Revue d'optique théorique et instrumentale.
[9] J. Hartmann, Zeit. für Instrumentenk. **24**, 1, p. 33 & 97, 1904.
[10] Y. Nakai, The Heavens, **48**, 503, p. 102~111, 1967. (In Japanese)